New "All-Acrylate" Block Copolymers: Synthesis and Influence of the Architecture on the Morphology and the Mechanical Properties

M. Jeusette,*,† Ph. Leclère,† R. Lazzaroni,† F. Simal,‡ J. Vaneecke,‡ Th. Lardot,‡ and P. Roose‡

Service de Chimie des Matériaux Nouveaux, Université de Mons-Hainaut, Place du Parc, 20, B-7000 Mons, Belgium, Research & Development, Cytec Surface Specialties, Anderlechtstraat 33, B-1620 Drogenbos, Belgium

Received July 18, 2006; Revised Manuscript Received December 6, 2006

ABSTRACT: Novel "all-acrylate" block copolymers have been synthesized by ATRP with a simple and cost-effective one-pot-two-step process. The $(A-B)_n$ copolymers are composed of an elastomer segment (A = P(2EHA-*co*-MA) = poly(2-ethylhexyl acrylate-*co*-methyl acrylate)) and a thermoplastic segment (B = PMMA = poly(methyl methacrylate)). To study the relationship between the molecular architecture and the mechanical properties, a four-arm radial block copolymer $(A-B)_4$ is compared to the linear diblock $(A-B)_1$ and symmetric triblock $(A-B)_2$ and compounds of similar composition. Atomic force microscopy (AFM) shows that all block copolymers present a well-defined microphase separation, which is confirmed by the observation of two glass transitions in DSC. Thermomechanical data from viscoelastic, indentation, and tensile measurements are discussed in terms of the structural characteristics of the copolymers. The increase in the complexity of the molecular structure results in an enhanced elastic response, and the stress−strain curves confirm the strengthening effect with increasing molecular connectivity (radial > linear triblock) and end-block length.

I. Introduction

Among the recent methods to control radical polymerizations (CRP), atom transfer radical polymerization (ATRP) has the potential to contribute to the need of new synthetic materials with improved properties for high-end applications.[1] Because of the versatility of ATRP, a wide range of polymer and (co)-polymers with complex compositions and architectures are now within reach.[2] In this context, pressure-sensitive adhesives (PSA) can be regarded as a typical application that could benefit from controlled radical polymerization of (meth)acrylates. Recently, however, it has been shown that for common polyacrylate compositions used in PSA's, narrow molecular mass distributions inherent to CRP do not lead to enhanced PSA performances due to the narrow Deborah window and the absence of strain hardening in elongation.[3] Alternatively, one can exploit another key feature of ATRP, i.e., the possibility to produce block copolymers. "All-acrylate" block copolymers prepared by different CRP processes have already been described and compared to the well-known styrenic block copolymers (SBC's) used in adhesive applications.[4] It has been argued that the use of (meth)acrylic building blocks provides better weather resistance in comparison to the unsaturated segments in SBC's and, in addition, also improves adhesion.[4,5]

An essential aspect of block copolymers with respect to adhesive formulation and PSA tailoring is the ability to generate well-defined microphase-separated structures for the selective mixing of additives, such as tackifying resins, into the rubbery elastomeric matrix.[6] The microscopic morphology of block copolymers plays a critical role in the mechanical properties of these materials.[7] When the separation of unlike segments in a block copolymer is driven by a net repulsion, the chemical junction between the blocks restricts the process to local segregation, i.e., on the scale of the chain length, leading to microphase-separated morphologies.

Direct synthesis of linear polymethacrylate-*block*-polyacrylate-*block*-polymethacrylate copolymers using ATRP is well-documented in the literature.[8] Recently, copolymers with radial architectures have gained much interest in academia and industry as a result of their attractive properties in terms of viscosity, degree of chain end functionality, processability, and mechanical performance, in comparison to their linear counterparts.[9] The preparation of radial polymers and block copolymers by ATRP has been reported by a few research groups and can be categorized along two approaches: (i) In the "arm-first" approach, linear "living" arms are reacted with multifunctional monomers, which upon coupling generate a microgel core structure. However, very long reaction times are usually needed to couple the multifunctional monomers. In addition, purification is usually required to remove the unreacted linear chains.[10] (ii) In contrast, the "core-first" strategy relies on the use of well-defined multifunctional initiators, from which chain growth takes place.[11]

In both cases, two steps are necessary to obtain the desired block copolymer. The one-pot synthesis of linear (meth)acrylic block copolymers using a sequential monomer addition method was first reported by Matyjaszewski.[8b] Here, the reaction still proceeds following a two-step mechanism, but there is no intermediate purification. Although this is a simple approach to the synthesis of block copolymers, the characterization of these copolymers has revealed significant deviation in terms of molecular dispersity, as compared to the materials obtained from a purified macroinitiator. Mechanical and rheological studies have also evidenced rather large discrepancies between the two types of compounds. Recently, Chen et al.[12] described a novel one-pot approach to prepare star polymers by ATRP. However, this procedure does not allow for the synthesis of block-type structures.

* Corresponding author. E-mail: melanie.jeusette@umh.ac.be. Telephone: +3265373865. Fax: +3265373861.

† Service de Chimie des Matériaux Nouveaux, Université de Mons-Hainaut.

‡ Research & Development, Cytec Surface Specialties.

10.1021/ma061613k CCC: $37.00
Published on Web 01/18/2007

Table 1. Description of the Block Copolymers[a]

sample	copolymer type
$(50-10)_1$	linear diblock
$(50-10)_2$	linear triblock
$(50-10)_4$	4-arm radial block
$(50-20)_4$	4-arm radial block

[a] The molecular weights (in kg mol^{-1}) of the segments expressed as $(A-B)_n$ are the expected values. The actual values are discussed in the Results Section.

Scheme 1. Sketch of the Block Copolymer Structures

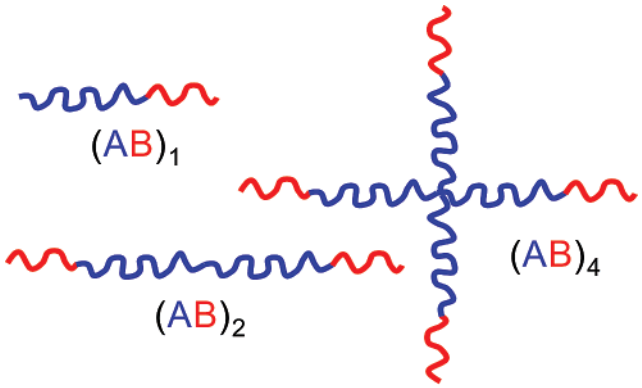

This paper reports on a study of the supramolecular ordering and the mechanical properties, as a function of composition and molecular structure, for new ATRP-derived linear and radial block copolymers prepared with a simple and cost-effective one-pot process. The primary goal of this work is a comparison between copolymers with similar composition but different chain architectures.[13] The structures of the block copolymers investigated here are presented in Table 1. The block copolymers are denoted as $(A-B)_n$, where A and B represent the elastomer segment (A = P(2EHA-*co*-MA) = poly(2-ethylhexyl acrylate-*co*-methyl acrylate)) and the thermoplastic segment (B = PMMA = poly(methyl methacrylate)), respectively. The index *n* relates to the structural arrangement, i.e., $n = 1$, 2, and 4 for a linear diblock, a linear triblock, and a four-arm radial block structure, respectively (cf. Scheme 1). The compositions of the copolymers were selected in the prospect of their final use as PSA. Generally, 2-ethylhexyl acrylate (2EHA) is considered as the main monomer, which usually accounts for more than 50% of the overall composition. Methyl acrylate (MA) was introduced as a regulating monomer for the adjustment of the glass-transition temperature. Throughout the study, the composition of the soft elastomeric segment was held constant at a 70/30 2EHA/MA ratio expressed as mass fraction. For the thermoplastic segments, methyl methacrylate (MMA) was used in order to promote phase separation, which is further controlled by the molar mass of the respective blocks. The selected units were finally composed of $\approx$ 50 kg mol^{-1} P(2EHA-*co*-MA)) and $\approx$ 10 kg mol^{-1} PMMA for the elastomer and thermoplastic sections, respectively. The length of the PMMA segments in the arms of the radial copolymer was also varied by preparing the radial $(50-20)_4$ compound. The phase-separated morphology, as evidenced by differential scanning calorimetry (DSC) and imaged by atomic force microscopy (AFM), is related to the mechanical properties measured with thermomechanical analysis (TMA), dynamical mechanical analysis (DMA), and tensile experiments.

II. Experimental Section

A. Copolymer Synthesis and Chemical Characterization. *Materials.* Pentaerythritol (99+%, Aldrich), 2-bromoisobutyryl bromide (98%, Aldrich), *N*,*N*′,*N*′,*N*″-pentamethyldiethylene-triamine (PMDETA; 99%, Aldrich), ethyl-2-bromoisobutyrate (initator **1**: 98%, Aldrich), diethyl *meso*-2,5-dibromoadipate (initiator **2**: 98%, Aldrich), and other reagents were commercially available and used without further treatment.

Chemical Analysis. Monomer conversion was determined by a Perkin-Elmer gas chromatograph (GC) equipped with a FID detector using a 30 m capillary column. Dodecane was used as an internal standard. The number-averaged (M_n) and the weight-averaged (M_w) molecular weight as well as the polydispersity index (M_w/M_n) were determined by size exclusion chromatography (SEC) using a Merck−Hitachi instrument (RI detector HP 1047A, Polymer Laboratories) in THF at 40 °C at a flow rate of 1 mL min^{-1}. Calibration was established with polystyrene standards (Polymer Laboratories). The copolymers exhibit compositional polydispersity and, hence, the polydispersity index values obtained from the chromatograms are merely approximations.

High-resolution proton-1 and carbon-13 NMR spectra were recorded on a Bruker Avance 300-DPX300 spectrometer in $CDCl_3$ at room temperature.

Polymerization Initiators. The chemical structure of the three initiators is depicted in Scheme 2. Note that the functionality *f* of the initiators **1**, **2**, and **3** is 1, 2, and 4, respectively. Whereas initiators **1** and **2** were used as supplied, initiator **3** (pentaerythritol tetrakis(2-bromoisobutyrate)) was synthesized according to Matyjaszewski et al.[15] Initiator **3** was characterized as follows: Yield: 62%; ^{1}H NMR, δ: 1.90 (s, 24H, C(Br)−CH_3), 4.35 (s, 8H, C−CH_2−O) ppm; ^{13}C NMR, δ: 31.1 (C(Br)−*C*H$_3$), 43.6 (*C*−CH$_2$−O), 54.8 (*C*(Br)−CH$_3$), 62.7 (C−*C*H$_2$−O), 170.7 (O−*C*═O) ppm.

Polymerizations. *Synthesis of Linear and Radial Random Copolymers.* Linear and radial P(2EHA-*co*-MA) elastomers were synthesized using ATRP. The procedure was typically as follows. First, CuBr and the initiator (**1**, **2**, or **3)** were purged three times with nitrogen gas cycles in a 100 mL Schlenk flask. Next, a degassed mixture of 2EHA, MA, dodecane, and toluene was transferred to the flask and then degassed PMDETA was added. Approximately 0.2 mL of solution was removed for analysis, and the flask was then placed in an oil bath at 90 °C while stirring. To follow the extent of the polymerization, samples were withdrawn from the reaction vessel at different time intervals for the determination of monomer conversion by GC and molecular weight growth by SEC. After synthesis, the polymer was diluted with toluene, filtered through a basic alumina column to remove the catalyst, and finally dried in vacuum at 85 °C for 12 h.

Synthesis of Linear and Radial Block Copolymers. The first step of the synthesis was similar to the procedure described before for the P(2EHA-*co*-MA) elastomers. Upon conversion of 2EHA and MA over 90%, deoxygenated MMA was added to the flask. The polymerization of the second step was subsequently run until more than 90% of MMA was consumed. Finally, the polymer was diluted in toluene, filtered through a basic alumina column to remove the catalyst, precipitated in methanol, filtered, and dried in vacuum at 85 °C for 12 h.

B. Thermal and Mechanical Analysis. *Film Preparation.* Films were prepared by casting a copolymer solution ($\approx$ 15 mg mL^{-1}, in toluene) in an aluminum dish covered with a silicone paper. The solvent was evaporated for 24 h at room temperature, and the samples were subsequently dried at 110 °C for approximately 2 h in order to remove any solvent traces. The film thickness was typically in the 300−500 μm range.

Differential Scanning Calorimetry (DSC). DSC curves were measured with a DSC Q10 (TA Instruments) at a linear heating rate of 20 °C/min. The sample mass was $\approx$10 mg.

Thermomechanical Analysis (TMA). Thermomechanical analysis was conducted in static penetration mode using a flat-ended indentation rod (radius = 1.27 mm) under a static normal load of 0.5 N. TMA data were recorded with a 2940 thermomechanical analyzer (TA Instruments) at a heating rate of 10 °C/min.

Dynamical Mechanical Analysis (DMA). Below room temperature, the linear viscoelastic properties were obtained by dynamical

Scheme 2. Chemical Structure of the Three Types of Initiator

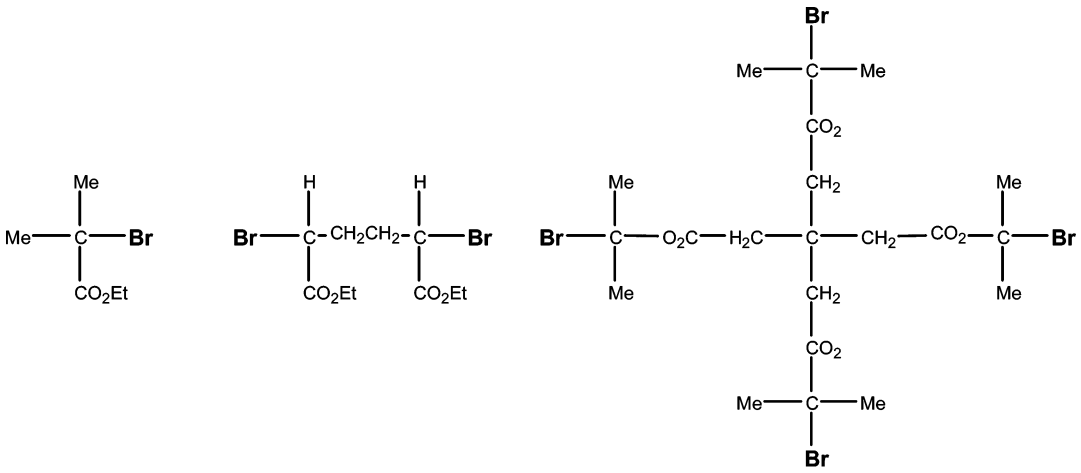

Initiator **1** Initiator **2** Initiator **3**

mechanical analysis in tensile deformation using a 2980 dynamic mechanical analyzer (TA Instruments). A strain oscillation with an amplitude of 0.1% was applied at a frequency of 1 Hz. For the temperature range from 30 to 180 °C, DMA data were recorded in oscillatory shear with a Paar-Physica UDS200 rheometer equipped with an electrically heated convection system. A parallel plate configuration (upper plate diameter = 25 mm) was used, and the strain oscillation was maintained at a frequency of 1 Hz with an amplitude of 1%. The temperature scanning rate was 3 °C/min for all the experiments. The linearity condition was verified at selected temperatures.

Uniaxial Stress−Strain Properties. Tensile properties were measured at room temperature with a Zwick Z010 elongation testing machine at a cross-head speed of 50 mm/min. For the tests, 3 cm × 1 cm rectangular-shaped specimens were cut from the solution-cast films. At least five independent measurements were performed for each sample.

C. AFM Imaging. The very low electronic contrast between the constitutive blocks of "all-acrylate" block copolymers is a major problem for the observation of nanophase-separated morphologies by transmission electron microscopy (TEM) and small-angle X-ray scattering (SAXS). As an alternative method, atomic force microscopy (AFM) is a suitable tool for the direct observation of phase separation in block copolymers.[14] Hence, the formation of the phase-separated microdomains in the solid state was observed by AFM and the results were related to the macroscopic mechanical and rheological properties measured independently.

Film Preparation. Thin films of the copolymers were prepared by solvent casting from a toluene solution (12 mg mL^{-1}) on freshly cleaved mica substrates. The thickness of the films (i.e., 700 ± 200 nm, as measured by ellipsometry) was chosen in order to make sure that: (i) the film surface is smooth (thicker films tend to be rougher and the topographic contrast can perturb the phase image), and (ii) the morphology is not affected by specific interactions with the substrate, as is often the case when the thickness is of the same order of magnitude as the microdomain size.[16] Because toluene is a good solvent for the investigated (meth)acrylate copolymers, selective precipitation was not expected to influence the morphology. The samples were first analyzed after complete evaporation of the solvent at room temperature. To investigate the effect of annealing on the surface morphology, the samples were heated at 140 °C, i.e., above the glass-transition temperature of the thermoplastic segments (PMMA), under high vacuum (10^{-7} Torr) for 24 h.

AFM Measurements. The AFM measurements were performed in "tapping mode" (TMAFM). In this mode, the cantilever holding the probe tip oscillates close to the resonance frequency (ca. 300 kHz) above the sample surface so that the tip is in intermittent contact with the surface at the lower end of the oscillation. This method minimizes the amount of energy transferred from the tip to the sample as compared to the contact-mode operation, where the tip is in permanent contact with the surface during scanning. The phase of the oscillating tip is very sensitive to the nature of the interaction with the surface. It has been shown that the phase lag can be directly related to the elastic modulus of the material when the amplitude is only slightly dampened upon contact with the surface.[17] Therefore, simultaneous acquisition of the phase and the height image provides a map of the local mechanical properties and allows the observation of phase-separated microdomains. All the AFM images were recorded with a Nanoscope IIIa microscope (Veeco, Inc) operated at room temperature in air using commercial cantilevers with a spring constant of 30 Nm^{-1}. Different areas of the same sample were inspected with scanning times of ca. 8 min. The images were digitally sampled at the maximum number of pixels (512) in each direction, and the Nanoscope image processing software was used for image analysis. Unless otherwise stated, image treatment was limited to a "flattening" operation, whereby a first-order surface representing height variations related to a possible tilt of the sample, is subtracted from the original image.

III. Results and Discussion

A. Polymer Synthesis. For the ATRP polymerizations in this study, the CuBr/PMDETA complex was used as the catalytic system because it is readily accessible and well-known to mediate the controlled polymerization of both acrylates and methacrylates.[18] The catalyst and the various initiators were found to be highly soluble in the reaction mixture at 90 °C. The first step in the sequential monomer addition approach followed here for the preparation of the block copolymers, consisted of the copolymerization of 2EHA and MA in a 70/30 weight ratio. Because no purification of the macroinitiator is

Table 2. Results of the First Copolymerization Step of 2EHA and MA Using Initiators 1, 2, and 3

initiator	*f*	$[M]_0$:$[\mathbf{I}]_0$:[catalyst]$_0$	reaction time (h)	2EHA/MA conversion (%)	$M_{n,theo}$ (kg mol^{-1})	$M_{n,SEC}$ (kg mol^{-1})	M_w/M_n (—)
1	1	364:1:1	23.3	95.6/96	48	54	1.3
2	2	728:1:2	21.3	95.7/95.6	96	57	1.7
3	4	1456:1:4	12.3	96.9/96.6	194	165	3.0

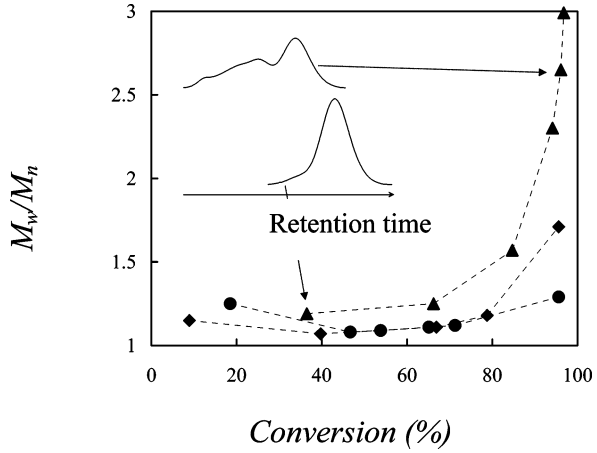

Figure 1. Plot of the polydispersity index vs monomer conversion for the ATRP synthesis of 2EHA/MA initiated by initiators **1**, **2**, and **3** (●, ◆, ▲), respectively. The SEC traces of the radial copolymer are shown for 37 and 95% conversion.

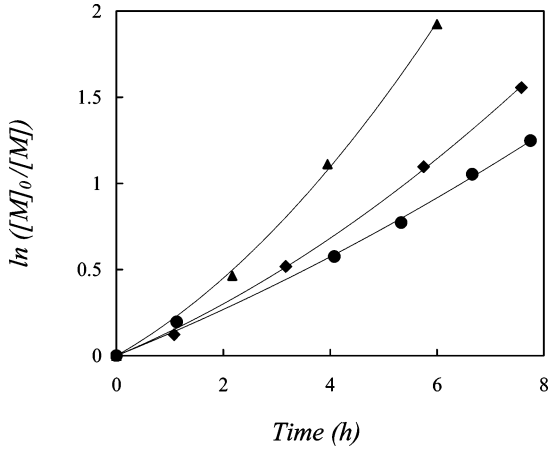

Figure 2. Kinetic plot for the ATRP of 2EHA initiated by initiators **1**, **2**, and **3** (●, ◆, ▲), respectively. The lines result from a second-order polynomial fit of the data.

carried out after the first step, it is a prerequisite to reach a high level of monomer conversion prior to the addition of the second-step monomer (i.e., MMA). In Table 2, the results of the first polymerization step are compared for a set of polymerizations with the three initiators. In this series, the ratio between the initial monomer and initiator concentrations, i.e., $[M]_0$:$[\mathbf{I}]_0$, was adjusted in order to get identical arm lengths starting from the different initiators. The target molecular weights were respectively 50, 100, and 200 kg mol^{-1}, and $M_{n,theo}$ expresses the expected molecular weight by taking into account the final monomer conversion.

The evolution of the polydispersity with monomer conversion for initiators **1**, **2**, and **3** (●, ◆, ▲) is depicted in Figure 1. In this plot, it is shown that in all cases, SEC traces remain narrow up to a conversion of ≈70%. Beyond this point, a broadening of the molecular weight distribution occurs for the three systems. Thus, for a conversion >95%, initiator **1** leads to a copolymer with a polydispersity of 1.3, whereas values larger than 1.5 are obtained with initiators **2** and **3** (1.7 and 3.0, respectively). On this basis, **1** can be considered as an efficient model initiator for the ATRP of 2EHA and MA. To the best of our knowledge, this constitutes the first example of "living" copolymerization of 2EHA and MA mediated by the CuBr/PMDETA catalytic system. The data clearly indicate that the extent of the broadening is related to the type of initiator. As already discussed by Gnanou et al.[10] in the case of the ATRP of styrene using a octafunctional initiator, this phenomenon can be related to coupling reactions between active radical species, the extent of such intermolecular coupling reactions being proportional to the number of arms present in the radial polymer. A comparison between the SEC traces of the radial copolymer (prepared with **3)** at 37 and 95% conversion (Figure 1) provides further support to the coupling hypothesis; at 95% conversion, the shoulders on the high molar mass side of the chromatogram are presumably due to the irreversible coupling of growing radicals. Note that in all cases the polymers remain completely soluble up to very high conversion levels. Although it was demonstrated by Matyjaszewski[16] that in the case of acrylates coupling reactions can be suppressed by proper adjustment of the reaction conditions, it is emphasized that the experimental conditions applied in this work were defined for subsequent extrapolation toward a fast, robust, and industrially viable process, which requires that high conversion be reached.

With initiator **1**, the concentration of the bromo-alkyl units was set at 1.1×10^{-2} mM. For initiators **2** and **3,** the concentrations were modified according to the functionality *f*, i.e., 5.0×10^{-3} and 2.5×10^{-3} mM, respectively. The ratio between the number of alkyl halide sites and catalyst was always kept constant (1:1). Hence, a constant polymerization rate R_p was expected for the three polymerizations according to the expression,

$$R_p = k_p K f [M][\mathbf{I}]_0 [Cu(I)Br]/[Cu(II)Br_2] \qquad (1)$$

where k_p is the rate constant, *K* is the ratio between the rate coefficients for the reversible activation and deactivation processes, and [Cu(I)Br] and [Cu(II)Br$_2$] are the concentrations of the catalytic redox pair.

The monomer consumption followed by GC and ^{1}H NMR did not indicate any significant deviation between the polymerization rate of 2EHA and MA. The ATRP kinetics of 2EHA with the different initiators are shown in Figure 2. It appears that the plot of ln($[M]_0$/[M]) versus time is nearly linear for initiator **1,** suggesting a constant concentration of radicals throughout the polymerization. However, a significant deviation from linearity is observed with initiators **2** and **3** when the monomer conversion exceeds ≈20%, and the kinetics is better described by a second-order polynomial equation. To our knowledge, only a few reports have been published on the kinetics of ATRP using multifunctional initiators. Under other similar reaction conditions, a decrease in polymerization rate was reported for the ATRP of styrene using an octafunctional initator, as compared to a monofunctional one.[10] A similar observation was made in the case of the ATRP of MMA using dendritic multifunctional initiators. Interestingly, in the latter work, an acceleration of the polymerization was also reported when a dodecafunctional initiator was used instead of a tetrafunctional one.[19] Still, in the case of the ATRP of *n*-butyl acrylate, Matyjaszewski et al.[15] did not observe any difference in the rates of polymerization between mono-, di-, tetra-, and hexafunctional initiators. Actually, for the reaction conditions mentioned in ref 15, no difference should really be expected. In the present case, the rate of polymerization seems to be related to the degree of branching of the growing copolymers. Since the pioneering work of Fischer, it is commonly recognized that the overall kinetic behavior is a product of several different rate constants and the dependence on various components does not necessarily conform to a first-order relationship.[20] Although ATRP seldom exhibits a gel effect, the branched nature of the polymer formed with initiator **3** causes the critical overlap concentration to be reached earlier during polymerization. Thus,

Table 3. Results of the Second Copolymerization Step of MMA Using Macroinitiators P1, P2, and P3 Prepared in the First Step

macroinitiator	f	$[M]_0$:[**P**]	reaction time (h)	MMA conversion (%)	$M_{n,theo}$ (kg mol^{-1})	$M_{n,SEC}$[24] (kg mol^{-1})	M_w/M_n (—)
P1	1	100:1	23.9	94.0	59.4	60	1.8
P2	2	200:1	25	90.7	118	72	2.1
P3	4	400:1	24.5	91.7	237	223	5.4
P4[a]	4	400:1	6.5	33.1		131	1.9

[a] Prepared with a purification step before PMMA polymerization.

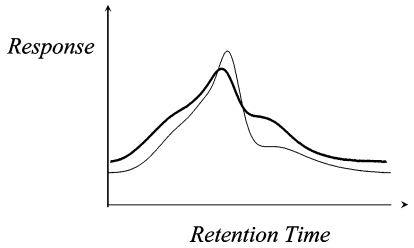

Figure 3. SEC traces (RI detector) before (normal trace) and after (thick trace) the second polymerization step using **P3** as macroinitiator.

a possible explanation for the observed trends could originate from the increased viscosity due to the formation of chain entanglements that hinder the diffusion of the macroradicals, which in turn causes a decrease in the rate of termination. Actually, the dependence of the termination rate coefficient on chain length and viscosity has been demonstrated in the past. The original model developed by Gilbert was accommodated for the CRP in the form of the following expression:[21]

$$k_t(\mathrm{DP}) = k_t(0)\mathrm{DP}^{-(0.65+0.02\mathrm{DP})}$$

Following the conditions developed for the first polymerization step, the addition of MMA was investigated for the preparation of block-type structures. Although the halogen exchange mechanism is known to improve the control over the polymerization,[22−23] the addition of a second load of catalyst at the second step increases the cost of the process and makes the purification of the final product more tedious, which is clearly not desirable in the prospect of upscaling. For these reasons, no additional catalyst was used in the second step of the reaction. Degassed MMA was added at the end of the first polymerization step (monomer conversion ≥95%), and the mixture was reacted until a high conversion of MMA was reached (≥90%). As a result of this sequential monomer addition process, a gradient copolymer of 2EHA, MA, and MMA is most likely formed at the early stage of the second step. In Table 3, the conditions and the results of the second step are given for the mono-, di-, and tetrafunctional macroinitiator. Obviously, MMA was largely converted during the polymerizations.

As can be seen from Figure 3, no major differences appear between the general shape of the SEC trace of the macroinitiator **P3** and the final block copolymer. Despite the relative complexity of the SEC traces, a shift toward higher molecular weight is observed. However, it can be noted that the second step of the polymerization does not seem to affect the molecular weight distribution to a large extent. This is likely due to the type of bimolecular termination which, in the case of MMA, mainly occurs by disproportionation because of the easily abstractable β-hydrogens.[25]

Although the reactions were carried out in small vessels using standard Schlenk techniques, upscaling (>1kg) of these polymerizations with industrial-grade monomers and solvents used without further purification (only oxygen removal through bubbling with nitrogen was applied) produced very similar results. It is therefore concluded that the present ATRP process can readily be scaled up for industrial production.

B. Phase Morphology. The base structural entity of the investigated block copolymers consists of an elastomer segment of ≈50 kg mol^{-1} and a thermoplastic segment of ≈10 kg mol^{-1}. The choice was not arbitrary but primarily guided by the performance of the materials as PSA after suitable formulation. It was observed that the linear triblock and especially the radial copolymer system perform very well with regard to cohesive and adhesive strength on both polar and nonpolar substrates. Aside from the chemical composition of the block segments, it is generally stated[26] that the block should be long enough in order to achieve good PSA properties, i.e., the soft segments should be entangled in order to act as an elastomer and the length of the hard blocks should be adjusted in order to get a well-separated microphase structure. Our rheological data indicate that the molecular weight between entanglements of the soft segments is ≈25 kg mol^{-1}. By synthesizing elastomer segments with molecular weights beyond this value, we comply with the first condition. To examine the formation of a microphase-separated structure, films of the block copolymers were analyzed by TMAFM.

For block copolymers, the presence of a phase-separated morphology can be evidenced from the phase images obtained in TMAFM. Here, no attempt was undertaken to analyze the absolute values of the phase signal; the vertical color scale of the phase images is chosen in order to produce the best contrast. Figure 4 shows typical AFM phase images observed for a sample of the linear diblock copolymer $(50-10)_1$.[27]

The film surface clearly shows an assembly of bright dots, i.e., areas where the phase lag is higher, dispersed in a dark matrix where the phase lag is lower. This is a clear signature of microphase separation, which is further supported by the observation of two glass transitions in DSC, one at low temperature associated to the elastomer part and one at high temperature corresponding to the thermoplastic part (cf. Table 5). Despite the polydispersity of this diblock copolymer, an ordered phase separation is observed. It is commonly accepted that molecular weight dispersity significantly reduces the microdomain order.[28]

However, Bendejacq et al.[29] recently reported well-ordered morphologies for a series of diblock copolymers with broad molecular weight distributions. A similar behavior is observed here. Because the phase shift is related to Young's modulus,[17] the bright spots can be assigned to PMMA, which is, at room temperature, harder than the elastomer segment constituted of P(2EHA-*co*-MA). Figure 4 (right) shows the phase image of the same linear diblock copolymer after annealing at 140 °C. The morphology is very similar to that observed before annealing. Yet, the dots are more regularly arranged in a well-defined hexagonal lattice, as indicated by the two-dimensional Fourier transform of the image. From the power spectrum of the images, the average center-to-center distance between dots is estimated to be 50 ± 5 nm. The AFM data clearly suggest a hexagonal arrangement of PMMA spheres in a P(2EHA-*co*-MA) matrix. The actual PMMA content for the diblock

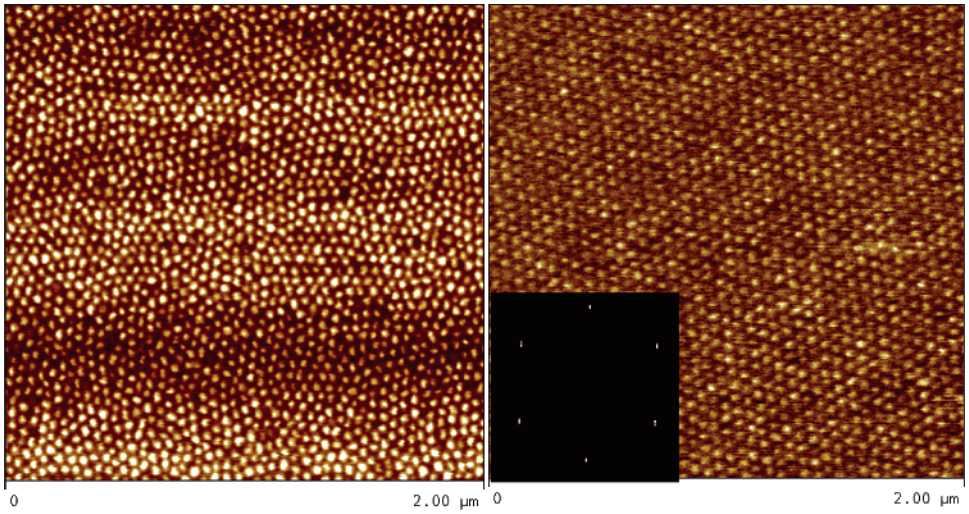

Figure 4. $2 \times 2\ \mu m^2$ TMAFM phase images of the $(50-10)_1$ diblock copolymer: before (left) and after (right) annealing at 140 °C. Inset: Fourier transform of the image showing the hexagonal symmetry of the lattice.

copolymer is ≈16 vol % according to the segmental composition, i.e., $(48-9.4)_1$. The morphology of this copolymer is in close agreement with our previous studies of the composition-morphology relationship in "all-acrylate" thermoplastic elastomers prepared by living anionic polymerization.[30] In this composition range, those copolymers indeed show a "spheres-in-a-matrix" morphology.

To determine the influence of the molecular architecture on the supramolecular ordering, the linear $(50-10)_2$ triblock and the linear $(50-10)_1$ diblock copolymer are compared. Figure 5 shows the morphology of the linear triblock copolymer at room temperature before and after annealing.

Before annealing, the phase image (Figure 5, top) shows a majority of round-shaped objects and a few elongated bright objects embedded in a dark continuous matrix. The elongated objects (4% of the objects) are attributed to PMMA rods partially oriented parallel to the surface. The width of those rods is 30 ± 5 nm, equal to the diameter of the round-shaped objects. The observed morphology suggests a collection of cylinders parallel and perpendicularly aligned to the surface. The prevalence of cylinders directed perpendicular to the surface after slow evaporation of the solvent (as with toluene) has clearly been demonstrated in previous studies of linear poly(meth)acrylate triblock copolymers.[30] Because the thermoplastic block has the highest surface free energy (42.5 mJ/m^2 for PMMA vs 36.1 mJ/m^2 for P(2EHA-*co*-MA)),[31] the material tends to organize so as to minimize the amount of PMMA at the surface by exposing only the apex of the PMMA cylinders. Hence, only a few elongated objects are visible on the AFM images. To confirm the existence of the cylindrical morphology, samples of the same copolymer were prepared in chloroform. As previously[30] demonstrated, the fast evaporation of chloroform during the film formation traps larger numbers of PMMA cylinders in the "flat" orientation. This is also verified here: the AFM image of a film prepared from chloroform (Figure 5, bottom) clearly shows the coexistence of perpendicular and flat cylinders at the surface and confirms that the morphology is indeed cylindrical. After annealing, all cylinders are directed normal to the surface and only their apex are visible (Figure 5, middle). The bright dots have an average diameter of 30 ± 5 nm, equal to that of the dots in Figure 5 (top). The spatial periodicity is fairly sharp, with an average distance of 60 ± 5 nm between the dots. A two-dimensional isotropic Fourier transform of the image (see Figure 5, inset) confirms the marked periodicity but reveals no further ordering at a larger length scale. The difference in morphology between the diblock (spherical) and the triblock (cylindrical) may be attributed to a deviation from the target composition for the triblock. Because the P(2EHA-co-MA) block is shorter than expected (see Table 2), the triblock copolymer might be richer in PMMA, which possibly drives the morphology toward a "cylinders-in-a-matrix" structure.

Nevertheless, it should be emphasized that, irrespective of the rather large polydispersity, this triblock copolymer also develops a well-defined phase-separated morphology.

Parts a and b of Figure 6 show AFM images obtained for the $(50-10)_4$ radial block copolymer and display a two-phase morphology of PMMA spheres dispersed in the P(2EHA-*co*-MA) matrix, in agreement with the two distinct glass transitions observed by DSC (vide infra);

Again, annealing results in a more regular spatial arrangements of the microdomain. The average center-to-center distance between the spheres is 50 ± 5 nm, i.e., the same value as for the diblock compound.[32] This four-armed radial copolymer has an actual composition of $(48.5-9.2)_4$, which corresponds to a PMMA content of ≈17 vol %. The observation of a spherical morphology similar to the linear diblock is thus fully consistent but the existence of a well-defined microphase separation for a copolymer with a polydispersity index exceeding 3 is quite remarkable.

To check the possible influence of the polydispersity on the microphase morphology, a second $(50-10)_4$ radial copolymer was synthesized by ATRP with the specific goal of obtaining a lower polydispersity. This synthesis was a two-step process in which, at each step, the polymerization was stopped at an early stage and the polymers were intensively purified in order to remove the residual monomers. For this second radial copolymer, the average number molecular weight and the polydispersity are 131 000 and 1.9, respectively. A single peak was observed in the SEC chromatogram, suggesting that coupling reactions were essentially avoided. The PMMA content was ≈17 vol %.

The AFM phase images (Figure 6c,d) show that both before or after annealing, the second, better defined radial block copolymer presents the same spherical morphology as the previous radial copolymer. The inset is a Fourier transform of the image, showing the hexagonal symmetry of the lattice. We can thus conclude that the polydispersity due to the presence

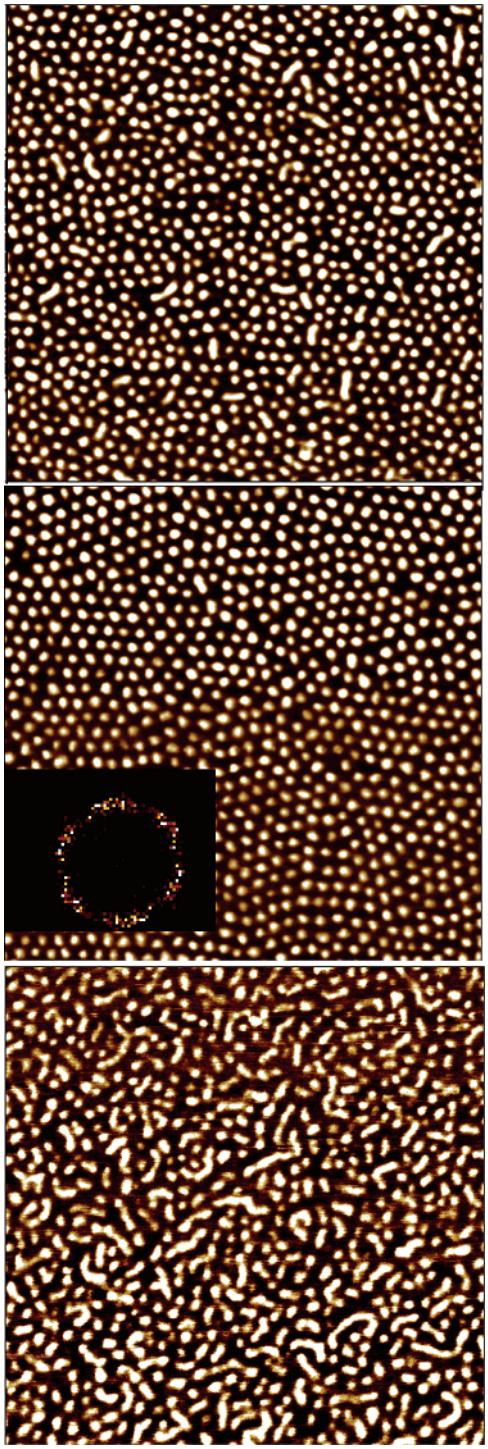

Figure 5. $2 \times 2\ \mu m^2$ TMAFM phase images of the $(50-10)_2$ linear triblock copolymer; samples prepared from toluene solutions: (top) before annealing, (middle) after annealing, (bottom) samples prepared from chloroform solutions.

of secondary species or coupled species does not much influence the solid-state microscopic morphology of the copolymer.

The AFM phase images (Figure 6e,f) of the $(50-20)_4$ radial block copolymer reveal a cylindrical morphology. Before annealing, flat cylinders (25% of the objects) coexist with bright dots whose diameter (30 ± 5 nm) is equal to the width of the flat cylinders. Again, the bright dots represent cylinders standing upright, perpendicular to the surface. After annealing, shorter segments of cylinders are aligned along the surface and their number is strongly reduced (only 12% of the bright objects). This corresponds to the expected behavior, i.e., the cylindrical PMMA domains reorient in order to expose their apex at the surface and to minimize the contact area with air. By comparing the two radial copolymers $(50-10)_4$ and $(50-20)_4$, it is concluded that a 2-fold increase of PMMA content leads to a spheres-to-cylinders morphological transition. This agrees with previous studies of linear di- and triblock copolymers,[28,30] showing a cylindrical morphology for PMMA contents >20 vol %.

As mentioned above, the phase separation for the copolymers is confirmed by DSC. The results listed in Table 4 show the presence of two glass-transition temperatures for all the block copolymer systems. The evidence of two distinct transitions points toward an amorphous two-phase microstructure. The T_g of the elastomer phase is similar for all of the block copolymers and corresponds to the values for the linear and radial P(2EHA-*co*-MA) copolymers of the same composition, i.e., $T_g \approx -40$ °C. In contrast, the high-T_g value of the $(50-10)_n$ block copolymers is sometimes lower than the T_g value of a PMMA homopolymer of molecular mass equivalent to that of the hard segments.

The most probable explanation for the T_g deviation is a composition drift of the thermoplastic microphase due to residual amounts of 2EHA monomer left after the first step and subsequently copolymerized during the second step of the synthesis. Similarly, a considerable decrease in the intensity and temperature of the glass transition assigned to the hard microdomains was reported for low-molecular-weight poly(MMA-*b*-2EHA-*b*-MMA)[33] and poly(MMA-*b*-*n*BA-*b*-MMA)[3] triblock copolymers prepared by living anionic polymerization. Partial segmental miscibility and the presence of a diffuse interlayer were invoked to account for those observations. In the present ATRP block copolymers, the composition gradient of the hard blocks may additionally promote miscibility and create a diffuse interphase (up to a pure PMMA phase beyond a critical molecular weight), thereby depressing the glass-transition temperature.

C. Thermomechanical Properties. The dynamic measurement of the small-strain viscoelastic properties over a wide temperature range is a convenient approach to determine the phase organization in segmented copolymers.[34,35] The AFM data have clearly shown that the copolymers present a phase separation, further supported by the DSC results. The viscoelastic data (Figure 7) show that the three copolymers ($(50-10)_1$, $(50-10)_2$, $(50-10)_4$) exhibit a major loss tangent peak centered at $T(\tan \delta_{max}) \approx -16$ °C, which is characteristic of the P(2EHA-*co*-MA) glass transition. The curve does not show a sharp peak typical for the second transition but rather a broad relaxation band. In particular, the diblock copolymer has a strong relaxation band around 45 °C. According to the DSC data, it would be straightforward to attribute this relaxation region to the glass transition of the thermoplastic domains. However, a contribution from an additional relaxation process is assumed to explain the large relaxation amplitude: as shown previously for linear styrenic[36,37] and polyacrylate block copolymers,[3] dangling or nontrapped chains may cause an increase of mechanical loss in the rubbery plateau region. Free elastomeric chains may be generated by termination during the first step of the synthesis, especially for the diblock system. Moreover, various authors[3,38] have demonstrated that the initiator-type in ATRP synthesis substantially affects the molecular mass distribution of MMA polymerization and that initiation by a brominated polyacrylate (i.e., P(2EHA-*co*-MA)) macroinitiator inherently leads to a broad molecular mass distribution of the PMMA segments.[3,38] Hence, it is suggested that free copolymer chains with short or no

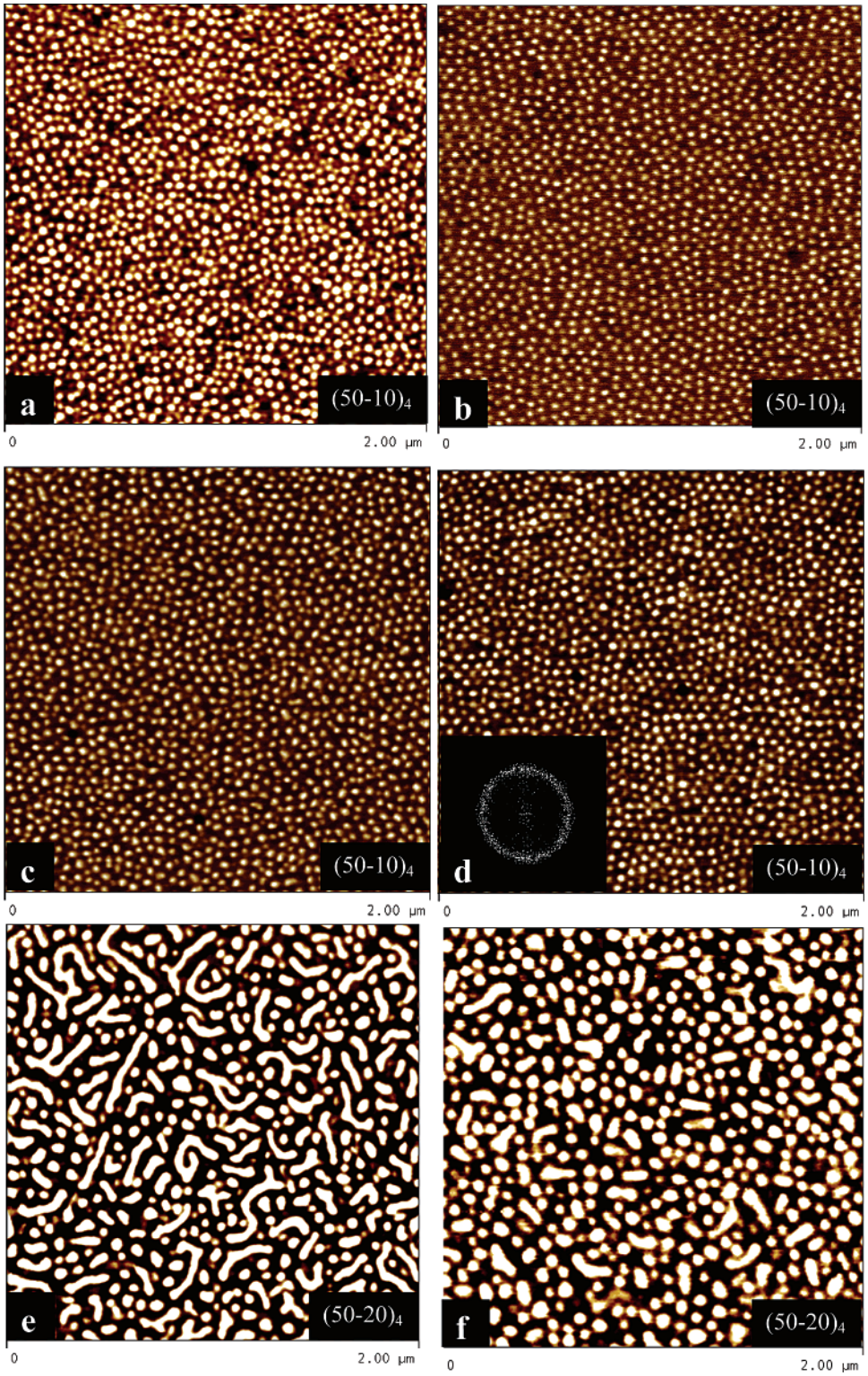

Figure 6. $2 \times 2\ \mu m^2$ TMAFM phase images of the $(50-10)_4$ radial block copolymer; samples prepared from toluene solutions: (a) before annealing, (b) after annealing. $2 \times 2\ \mu m^2$ TMAFM phase images of the "new" $(50-10)_4$ radial copolymer: before (c) and after (d) annealing at 140 °C and $2 \times 2\ \mu m^2$ TMAFM phase images of the $(50-20)_4$ radial block copolymer; samples prepared from toluene solutions: (e) before annealing, (f) after annealing.

PMMA segments (i.e., not physically cross-linked in the microdomains) impart an amplified loss to the diblock copolymer, acting as a diluent of the entangled matrix. In Figure 7, the features of the G' and tan δ profiles for the linear triblock $(50-10)_2$ and the radial $(50-10)_4$ block copolymers are similar to the diblock system, i.e., revealing an extended relaxation domain between 10 and 110 °C and no transition related to the hard domains. The connectivity of the elastic network results in an increase of G'. In addition, it seems to limit the relaxation due to dangling chains or branches (the presence of nontrapped chains being less probable in these systems), as concluded from the reduction of the intermediate loss tangent peak. It is noteworthy that the viscoelastic response of the linear triblock $(50-10)_2$ is very close to the linear ATRP poly(MMA-*b*-*n*BA-*b*-MMA) system ($(25-9)_2$ in our notation) studied by Tong et al.,[3] and the present results corroborate their conclusions.

Table 4. T_g (DSC) of Homo- and Block Copolymers

	T_g (°C)	
sample	A	B
linear P(2EHA-*co*-MA)	−41	
radial P(2EHA-*co*-MA)	−40	
linear PMMA		102
$(50-10)_1$	−41	73
$(50-10)_2$	−39	59
$(50-10)_4$	−39	98
$(50-20)_4$	−40	103

The viscoelastic data show that when the molecular mass of the radial end blocks is increased, a reinforcing (filling) effect is observed through the enhancement of the elastic modulus in the rubbery plateau region (Figure 7a). A weak transition characteristic of the glass transition of PMMA becomes apparent at 130 °C in the tan δ profile, and the viscoelastic relaxation domain at intermediate temperatures is significantly reduced (Figure 7b), presumably as a result of the low number of dangling chain arms. The thermomechanical analysis of the "new" radial $(50-10)_4$ copolymer also shows the disappearance of that intermediate relaxation domain, consistent with its better-defined molecular structure, which is expected to improve the elastic properties.

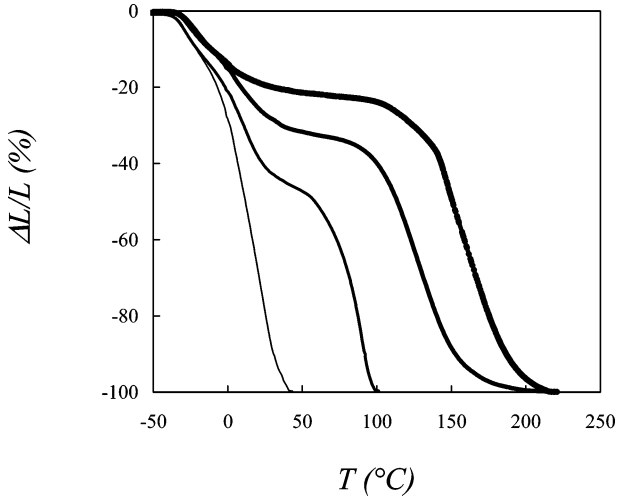

Figure 8. TMA indentation profiles for the series of copolymers $(50-10)_1$ (diblock), $(50-10)_2$ (triblock), $(50-10)_4$ (radial), and $(50-20)_4$ (radial) represented with lines of increasing thickness, respectively.

The TMA data shown in Figure 8 provide further indications with regard to the phase behavior of the block copolymers $(A-B)_n$. For the diblock system, two consecutive penetration steps

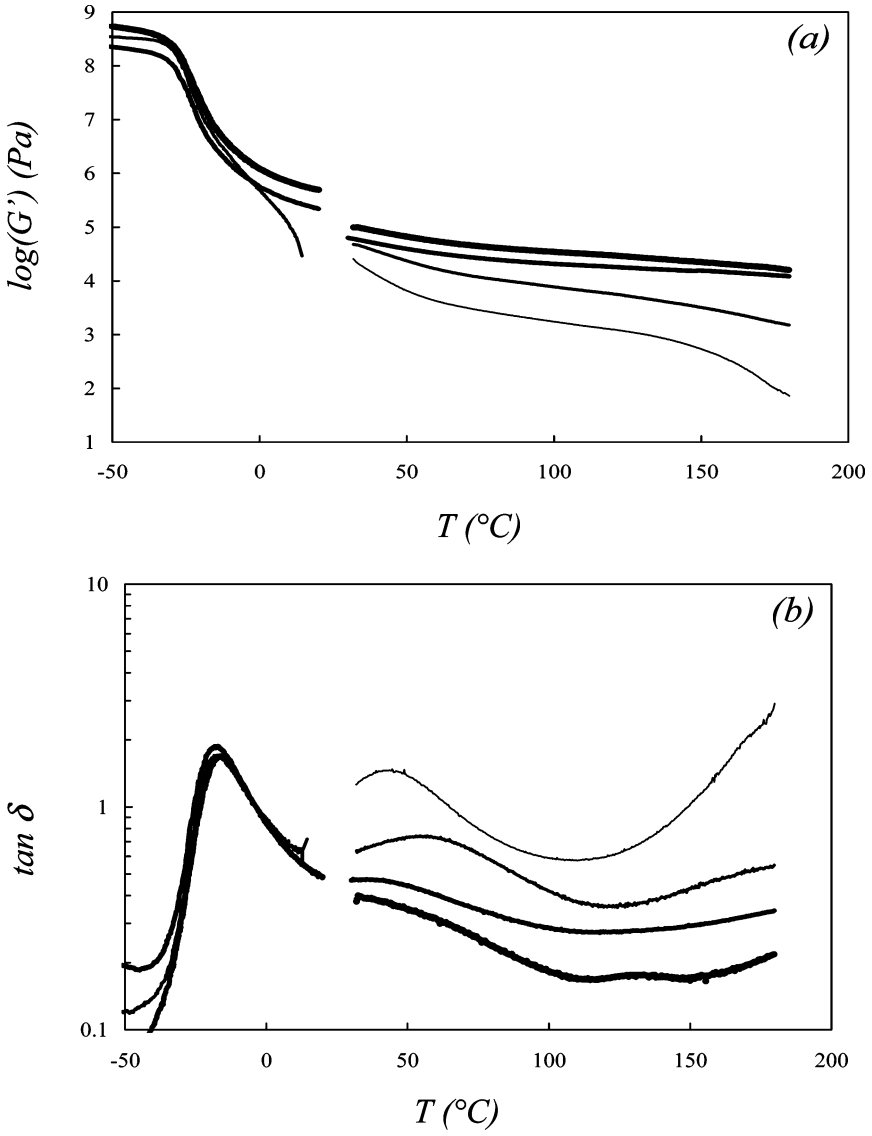

Figure 7. (a) Storage modulus and (b) loss tangent (tan δ) as a function of temperature for the series of copolymers $(50-10)_1$ (diblock), $(50-10)_2$ (triblock), $(50-10)_4$ (radial), and $(50-20)_4$ (radial) represented with lines of increasing thickness, respectively.

Table 5. TMA Data

sample	$T_{on,1}$ (°C)	$T_{on,2}$ (°C)	indentation at 50 °C (%)
$(50-10)_1$	−34		100
$(50-10)_2$	−35	74	47
$(50-10)_4$	−31	103	32
$(50-20)_4$	−32	133	21

Table 6. Ultimate Tensile Properties

sample	ultimate tensile strength (MPa)	elongation at break (%)
$(50-10)_2$	0.6	440
$(50-10)_4$	1.3	480
$(50-20)_4$	2.9	305

without an intermediate plateau are visible under the applied load. A temperature plateau appears for the linear triblock copolymer, which becomes even more marked for the radial copolymer. In addition, the indentation in the rubbery plateau region decreases with increasing *n*-value and essentially reflects the higher elastic character of the elastomer phase. When increasing the length of the outer block segments, the indentation plateau is further extended toward higher temperatures. Table 5 summarizes the temperatures at penetration onset in the TMA profiles, T_{on}, as well as the relative indentation at 50 °C. There is a good agreement between the glass-transition temperatures reported by DSC and the onset temperatures, T_{on}, determined by TMA. The major softening points for the linear $(50-10)_2$ triblock and the radial systems are presumably related to the glass transition of the end blocks. The penetration level at 50 °C reflects the increase of Young's modulus due to the increasingly constrained architecture of the core elastomer.

The ultimate properties of the radial branched blocks and the related linear triblock $(50-10)_2$ are reported in Table 6. The other materials could not be handled properly at room temperature. The data clearly reveal the strengthening effect due to the radial structure as well as the end block length.

IV. Synopsis

With the aim to study the relation between the macromolecular architecture, the microphase morphology and the mechanical properties, a series of (2EHA-*co*-MA)-*block*-MMA copolymers was prepared by ATRP either as linear diblocks, symmetric linear triblocks, or symmetric four-arm radial structures. The synthetic process was designed for subsequent application at an industrial scale.

The TMAFM results obtained on solution-cast thin films clearly show microphase-separated morphologies. A remarkable conclusion of this work is that those well-defined morphologies are present even in block copolymers with nonideal structures, i.e., with broad polydispersity. Comparison with a compound with a better-defined molecular structure shows no significant morphological differences. The DSC results confirm the phase separation observed by AFM. In some cases, the temperature of the glass transition ascribed to the hard domains is lower than the value for a PMMA homopolymer of equivalent molecular mass. This is attributed to a composition gradient that promotes miscibility and possibly creates a diffuse interphase.

The conditions of the synthetic route applied here have been design in the perspective of upscaling. As a drawback, they lead to the generation of copolymers or copolymer segments that partially or even do not participate in the physical (microphase) network (e.g., copolymers with no or very short PMMA blocks). This has a drastic effect on the viscoelastic behavior of the materials, which reveals a broad intermediate damping region for all the block copolymers. The damping amplitude is apparently related to the motional constraints imposed by the copolymer structure. Hence, the mechanical damping is attributed to the relaxation of dangling or free polymers chains within the physical network.

That problem is solved by using a radial architecture of PMMA segments of appropriate length.

The TMA data show that the molecular complexity of the acrylate block copolymers results in an enhanced elastic response, and the stress−strain curves confirm the strengthening effect with increasing molecular connectivity (radial > linear triblock) and end-block length.

From the observed microscopic morphology and the mechanical properties, it can be expected that the radial block copolymers described herein should behave as valuable polymer bases for PSA applications. Preliminary work has shown that adequate formulation with these polymers indeed leads to quite remarkable adhesive performances.[39]

Acknowledgment. We thank M. Voué (Materia-Nova, Mons) for the ellipsometry measurements. Research in Mons is partly supported by the Inter-University Attraction Pole Program of the Belgian Federal Science Policy PAI(V-3), the European Commission, the Government of the Region of Wallonia (Phasing Out-Hainaut), and the Belgian National Fund for Scientific Research FNRS/FRFC. Ph.L. is Research Associate of FNRS (Belgium).

References and Notes

(1) Matyjaszewski K. In *Controlled/Living Radical Polymerization*; ACS Symposium Series 768; Spanswick, J., Branstetter, E. A., Huber, W. F., Eds.; American Chemical Society: Washington, D.C., 2000; Chapter 30, pp 427.
(2) Davis, K. A.; Matyjaszewski, K. *Adv. Polym. Sci.* **2002**, *159*, 2.
(3) Lakrout, H.; Creton, C.; Ahn, D.; Shull, K. R. *Macromolecules* **2001**, *34*, 7448.
(4) (a) Tong, J. D.; Moineau, G.; Leclère, Ph.; Brédas, J. L.; Lazzaroni, R.; Jérôme, R. *Macromolecules* **2000**, *33*, 470. (b) Tong, J. D.; Jérôme, R. *Polymer* **2000**, *41*, 2499.
(5) Yamamoto, M.; Nakano, F.; Doi, T.; Moroishi, Y. *Int. J. Adhes. Adhes.* **2002**, *22*, 37.
(6) Jagisch, F. C.; Tancrede, J. M. *Handbook of Pressure Sensitive Adhesive Technology*, 3rd ed.; D. Satas, D., Ed.; Van Nostrand Reinhold: New York, 1999, Chapter 16, pp 346.
(7) *Thermoplastic Elastomers*: *A Comprehensive Review*; Legge, N. R., Holden, G., Schroeder, E., Eds.; Hanser Publishers: New York, 1987.
(8) (a) Shipp, D. A.; Wang, J.-L.; Matyjaszewski, K. *Macromolecules* **1998**, *31*, 8005. (b) Matyjaszewski, K.; Shipp, D. A.; McMurtry, G. P.; Gaynor, S. G.; Pakula, T. *J. Polym. Sci., Part A: Polym. Chem.* **2000**, *38*, 2023.
(9) (a) Mishra, M. K.; Kobayashi, S. *Star and Hyperbranched Polymers;* Marcel Dekker: New York, 1999. (b) Shim, J. S.; Kennedy, J. P. *J. Polym. Sci., Part A: Polym. Chem.* **1999**, *37*, 815. (c) Puskas, J. E.; Antony, P.; Kwon, Y.; Paulo, C.; Kovar, M.; Norton, P. R.; Kaszas, G.; Altstädt, V. *Macromol. Mater. Eng.* **2001**, *286*, 565.
(10) (a) Xia, J.; Zhang, X.; Matyjaszewski, K. *Macromolecules* **1999**, *32*, 4482. (b) Zhang, X.; Xia, J.; Matyjaszewski, K. *Macromolecules* **2000**, *33*, 2340. (c) Baek, K. Y.; Kamigaito, M.; Sawamoto, M. *Macromolecules* **2001**, *34*, 215.
(11) (a) Wang, J. S.; Greszta, D.; Matyjaszewski, K. *Polym. Mater. Sci. Eng.* **1995**, *73*, 416. (b) Ueda, J.; Kamigaito, M.; Sawamoto, M. *Macromolecules* **1998**, *31*, 6762. (c) Angot, S.; Shanmugananda Murthy, K.; Taton, D.; Gnanou, Y. *Macromolecules* **1998**, *31*, 7218. (d) Matyjaszewski, K.; Miller, P. J.; Pyun, J.; Kickelbick, G.; Diamanti, S. *Macromolecules* **1999**, *32*, 6526. (e) Matyjaszewski, K. *Polym. Int.* **2003**, *52*, 1559. (f) Mei, L.; Ke, M.; Matyjaszewski, K.; *Macromolecules* **2004**, *37*, 2106. (g) Mei, L.; Nazeem, M. J.; Ke, M.; Matyjaszewski, K. *Macromolecules* **2004**, *37*, 2434. (h) Ke, M.; Haifeng, G.; Matyjaszewski, K. *J. Am. Chem. Soc.* **2005**, *127*, 3825.
(12) Deng, G.; Chen, Y. *Macromolecules* **2004**, *37*, 18.
(13) The average molecular weight of polymers made by a well-controlled ATRP can be determined from the ratio of consumed monomer to initiator. In this work, the volume content of PMMA was calculated

from M_n defined from the degree of polymerization and the conversion according to the following references: Matyjaszewski, K.; Jianhui, X. *Chem. Rev.* **2001**, *101*, 2921; Grimaud, T.; Matyjaszewski, K. *Macromolecules* **1997**, *30*, 2216, and density values of PMMA, PMA, and P(2EHA) bulk polymers reported in *Polymer Handbook*, 3rd ed.; Brandrup, J., Immergut, E. H., Eds.; John Wiley and Sons: New York, 1989.

(14) (a) Coulon, G.; Collin, B.; Ausserre, D.; Chatenay, D.; Russell, T. P. *J. Phys. Fr.* **1990**, *51*, 2801. (b) Collin, B.; Chatenay, D.; Coulon, G.; Ausserre, D.; Gallot, Y. *Macromolecules* **1992**, *25*, 1621. (c) van den Berg, R.; de Groot, H.; van Dijk, M. A.; Denley, D. R. *Polymer* **1994**, *35*, 5778. (d) Leclère, Ph.; Lazzaroni, R.; Brédas, J. L.; Yu, J. M.; Dubois, Ph.; Jérôme, R. *Langmuir* **1996**, *12*, 4317. (e) Tong, J. D.; Leclère, Ph.; Doneux, C.; Brédas, J. L.; Lazzaroni, R.; Jérôme, R. *Polymer* **2001**, *42*, 3503.

(15) Matyjaszewski, K.; Miller, P. J.; Pryun, J.; Kickelbick, G.; Diamanti, S. *Macromolecules* **1999**, *32*, 6526.

(16) (a) Hashimoto, T.; Nagatoshi, K.; Todo, A.; Hasegawa, H.; Kawai, H.; *Macromolecules* **1974**, *7*, 364. (b) Hashimoto, T.; Todo, A.; Itoi, H.; Kawai, H. *Macromolecules* **1977**, *10*, 377. (c) Todo, A.; Kiuno, H.; Miyoshi, K.; Hashimoto, T.; Kawai, H. *Polym. Eng. Sci.* **1977**, *17*, 587. (d) Gallot, B. R. M. *Adv. Polym. Sci.* **1978**, *29*, 85. (e) Gallot, B. In *Liquid Crystalline Order in Polymers*; Blumstein, A., Ed.; Academic Press: New York, 1978; p 223. (f) Hashimoto, T.; Shibayama, M.; Kawai, H. *Macromolecules* **1980**, *13*, 1237. (g) Hashimoto, T.; Fujimura, M.; Kawai, H. *Macromolecules* **1980**, *13*, 1660. (h) Thomas, E. L.; Anderson, D. M.; Henkee, C. S.; Hoffman, D. *Nature* **1988**, *334*, 598. (i) Riess, G.; Bahhadur, P. In *Encyclopedia of Polymer Science and Engineering*; Mark, H. F., Bikales, N. M., Overberger, C., G.; Menges, G., Eds.; Wiley: New York, 1989; p 324.

(17) (a) Bar, G.; Thomman, Y.; Brandsch, R.; Cantow, H. J.; Whangbo, M. H. *Langmuir* **1997**, *13*, 3807. (b) Magonov, S. N.; Elings, V.; Whangbo, W. H. *Surf. Sci. Lett.* **1997**, *375*, 385. (c) Burnham, N. A.; Behrend, O. P.; Oulevey, F.; Gremaud, G.; Gallo, P.-J.; Gourdon, D.; Dupas, E.; Kulik, A. J.; Pollock, H. M.; Briggs, G. A. D. *Nanotechnology* **1997**, *8*, 67.

(18) Matyjaszewski, K.; Gobelt, B.; Paik, H.-J.; Horwitz, C. P. *Macromolecules* **2001**, *34*, 430.

(19) Hovestad, N. J.; van Koten, G.; Bon, S. A. F.; Haddleton, D. M. *Macromolecules* **2000**, *33*, 4048.

(20) Fischer, H. *Macromolecules* **1997**, *30*, 5666.

(21) Shipp, D. A.; Matyjaszewski, K. *Macromolecules* **1999**, *32*, 2948.

(22) Li, M.; Jahed, N. M.; Min, K.; Matyjaszewski, K. *Macromolecules* **2004**, *37*, 2434.

(23) Matyjaszewski, K.; Shipp, D. A.; Wang, J.-L.; Grimaud, T.; Patten, T. E. *Macromolecules* **1998**, *31*, 6836.

(24) The values of M_n and M_w were verified by SEC with multiple-angle light scattering detection (MALS). P1 and P2 showed a normal elution behaviour with $M_n = 56$ kg mol^{-1} and $M_w/M_n = 1.4$ for P1, and $M_n = 79$ kg mol^{-1} and $M_w/M_n = 2.1$ for P2, in excellent agreement with the values reported in Table 4. However, the radial copolymer P3 showed abnormal elution behaviour characteristic of highly branched molecules. No reliable molar mass data could be obtained in this case.

(25) Yamada, B.; Zetterlund, P. B. In *Handbook of Radical Polymerization*; Matyjaszewski, K., Davis, T. P., Eds.; John Wiley & Sons: New York, 2002; Chapter 3, p 117.

(26) Benedek, I.; Heymans, L. J. In *Pressure-Sensitive Adhesives Technology*; Marcel Dekker: New York, 1997.

(27) For the sake of simplicity, the copolymers are referred to in the discussion with the names defined in Table 1 rather than with the actual molecular weights.

(28) Leclère, Ph.; Moineau, G.; Minet, M.; Dubois, P.; Jérôme, R.; Brédas, J. L.; Lazzaroni, R. *Langmuir* **1999**, *15*, 3915.

(29) Bendejacq, D.; Ponsinet, V.; Joanicot, M.; Loo, Y. -L.; Register, R. A. *Macromolecules* **2002**, *35*, 6645.

(30) (a) Tong, J. D.; Leclère, Ph.; Rasmont, A.; Brédas, J. L.; Lazzaroni, R.; Jérôme, R. *Macromol. Chem. Phys.* **2000**, *201*, 1250. (b) Tong, J. D.; Leclère, Ph.; Doneux, C.; Brédas, J. L.; Lazzaroni, R.; Jérôme, R. *Polymer* **2000**, *41*, 4617. (c) Rasmont, A.; Leclère, Ph.; Doneux, C.; Lambin, G.; Tong, J. D.; Jérôme, R.; Brédas, J. L.; Lazzaroni, R. *Colloids Surf. B: Biointerfaces* **2000**, *19*, 381.

(31) Van Krevelen, D. W. *Properties of Polymers*, 3rd ed.; Elsevier: Amsterdam, 1990.

(32) We have checked that the morphology is indeed spherical by analyzing samples of the radial copolymer deposited from chloroform. The corresponding AFM images (not shown here) are very similar to those obtained from toluene, confirming the absence of cylindrical PMMA domains.

(33) Jérome, R.; Bayard, Ph.; Fayt, R.; Jacobs, Ch.; Varshney, S.; Teyssié, Ph. In *Thermoplastic Elastomers*, 2nd ed.; Holden, G., Legge, N. R., Quirk, R., Schroeder, E., Eds.; Hanser: Munich, 1996; p 521.

(34) Ferry, J. D. In *Viscoelastic Properties of Polymers*, 2nd ed.; Wiley: New York, 1970.

(35) Hale, A.; Bair, H. E. In *Thermal Characterization of Polymeric Materials*, 2nd ed.; Turi, E. A., Ed.; Academic Press: San Diego, 1981.

(36) Berglund, C. A.; Mckay, K. W. *Polym. Eng. Sci.* **1993**, *33*, 1195.

(37) Mckay, K. W.; Gros, W. A.; Charles, F. D. *J. Appl. Polym. Sci.* **1995**, *56*, 947.

(38) Moineau, C.; Minet, M.; Teyssié, P.; Jérome, R. *Macromolecules* **1999**, *32*, 8277.

(39) Simal, F.; Tweedy, H.; Van Es, S.; Roose, P. UCB Patent EP1433799, 2004.

MA061613K